

Article

Crystal-Chemistry of Sulfates from the Apuan Alps (Tuscany, Italy). VII. Magnanelliite, $K_3Fe^{3+}_2(SO_4)_4(OH)(H_2O)_2$, a New Sulfate from the Monte Arsiccio Mine

Cristian Biagioni ^{1,*}, Luca Bindi ²  and Anthony R. Kampf ³¹ Dipartimento di Scienze della Terra, Università di Pisa, Via Santa Maria 53, I-56126 Pisa, Italy² Dipartimento di Scienze della Terra, Università degli Studi di Firenze, Via G. La Pira 4, I-50121 Firenze, Italy; luca.bindi@unifi.it³ Mineral Sciences Department, Natural History Museum of Los Angeles County, 900 Exposition Boulevard, Los Angeles, CA 90007, USA; akampf@nhm.org

* Correspondence: cristian.biagioni@unipi.it; Tel.: +39-050-221-5789

Received: 22 November 2019; Accepted: 10 December 2019; Published: 12 December 2019



Abstract: The new mineral species magnanelliite, $K_3Fe^{3+}_2(SO_4)_4(OH)(H_2O)_2$, was discovered in the Monte Arsiccio mine, Apuan Alps, Tuscany, Italy. It occurs as steeply terminated prisms, up to 0.5 mm in length, yellow to orange-yellow in color, with a vitreous luster. Streak is pale yellow, Mohs hardness is ca. 3, and cleavage is good on {010}, fair on {100}. The measured density is 2.82(3) g/cm³. Magnanelliite is optically biaxial (+), with $\alpha = 1.628(2)$, $\beta = 1.637(2)$, $\gamma = 1.665(2)$ (white light), $2V_{meas} = 60(2)^\circ$, and $2V_{calc} = 59.9^\circ$. It exhibits a strong dispersion, $r > v$. The optical orientation is $Y = \mathbf{b}$, $X \wedge \mathbf{c} \sim 25^\circ$ in the obtuse angle β . It is pleochroic, with $X =$ orange yellow, Y and $Z =$ yellow. Magnanelliite is associated with alum-(K), giacovazzoite, gypsum, jarosite, krausite, melanterite, and scordariite. Electron microprobe analyses give (wt.%): SO_3 47.82, TiO_2 0.05, Al_2O_3 0.40, Fe_2O_3 25.21, MgO 0.07, Na_2O 0.20, K_2O 21.35, H_2O_{calc} 6.85, total 101.95. On the basis of 19 anions per formula unit, assuming the occurrence of one $(OH)^-$ and two H_2O groups, the empirical chemical formula of magnanelliite is $(K_{2.98}Na_{0.04})_{\Sigma 3.02}(Fe^{3+}_{2.08}Al_{0.05}Mg_{0.01})_{\Sigma 2.14}S_{3.93}O_{16}(OH)(H_2O)_2$. The ideal end-member formula can be written as $K_3Fe^{3+}_2(SO_4)_4(OH)(H_2O)_2$. Magnanelliite is monoclinic, space group $C2/c$, with $a = 7.5491(3)$, $b = 16.8652(6)$, $c = 12.1574(4)$ Å, $\beta = 94.064(1)^\circ$, $V = 1543.95(10)$ Å³, $Z = 4$. Strongest diffraction lines of the observed X-ray powder pattern are [d (in Å), estimated visual intensity, hkl]: 6.9, medium, 021 and 110; 4.91, medium-weak, 022; 3.612, medium-weak, $\bar{1}32$, 023, and $\bar{1}13$; 3.085, strong, 202, 150, and $\bar{1}33$; 3.006, medium, 004, $\bar{1}51$, and 151; 2.704, medium, 152 and $\bar{2}23$; 2.597, medium-weak, $\bar{2}42$; 2.410, medium-weak, 153. The crystal structure of magnanelliite has been refined using X-ray single-crystal data to a final $R_1 = 0.025$, on the basis of 2411 reflections with $F_o > 4\sigma(F_o)$ and 144 refined parameters. The crystal structure is isotypic with that of alcaparrosaite, $K_3Ti^{4+}Fe^{3+}(SO_4)_4O(H_2O)_2$.

Keywords: magnanelliite; new mineral species; sulfate; Raman spectroscopy; crystal structure; alcaparrosaite; Monte Arsiccio mine; Apuan Alps; Italy

1. Introduction

The occurrence of secondary sulfate assemblages in the pyrite ores from the Apuan Alps (Tuscany, Italy) was reported in the second half of the nineteenth Century (e.g., D'Achiardi [1]). However, few species were reported, and, among them, some were doubtful. For instance, D'Achiardi [1] reported the presence of gypsum, melanterite, halotrichite, alum-(K), goslarite, and, possibly, coquimbite. Since the second half of the 2000 s, the mineralogical study of the pyrite ± baryte ± iron oxide ore deposits

from the southern Apuan Alps allowed the identification of some interesting sulfate assemblages, in which rare or even new mineral species were identified. The Fornovolasco ore deposit was the first locality to be studied using modern analytical techniques. Here, Biagioni et al. [2] described the new oxy-hydroxy iron sulfate volaschioite, $\text{Fe}^{3+}_4\text{O}_2(\text{SO}_4)(\text{OH})_6 \cdot 2\text{H}_2\text{O}$. Later, Mauro et al. [3] identified a new hydrated iron phosphate-sulfate from the Buca della Vena mine, naming it bohoslavite, $\text{Fe}^{3+}_4(\text{PO}_4)_3(\text{SO}_4)(\text{OH})(\text{H}_2\text{O})_{10} \cdot n\text{H}_2\text{O}$. The most recent discovery is a sulfate assemblage found at the Monte Arsiccio mine, in which well-crystallized sulfate specimens were recovered, including three new mineral species, i.e., giacovazzoite [4], scordariite [5], and magnanelliite.

Magnanelliite was identified on a specimen found by the mineral collector Mario Bianchini. The name honors Stefano Magnanelli (b. 1959), chemist and mineral collector, for his contributions to the knowledge of the mineralogy of the Apuan Alps hydrothermal veins. He coauthored the type description of bottinoite [6] and provided the first specimens of parasterryite [7] and bianchiniite [8], as well as several samples from the Carrara marble quarries and other mining sites of the Apuan Alps, supporting the mineralogical studies of these occurrences. The mineral and its name have been approved by the Commission on New Minerals, Nomenclature and Classification of the International Mineralogical Association (IMA 2019-010). The holotype specimen of magnanelliite is deposited in the mineralogical collection of the Museo di Storia Naturale, Università di Pisa, Via Roma 79, Calci (Pisa), Italy, under catalog number 19894. A cotype specimen is deposited in the collections of the Natural History Museum of Los Angeles County, 900 Exposition Boulevard, Los Angeles, CA 90007, USA, under catalogue number 67241.

This paper presents the definition, occurrence, and crystal structure of the new mineral species magnanelliite.

2. Occurrence and Physical Properties

The Monte Arsiccio mine (latitude 43°58'N, longitude 10°17'E) exploited a pyrite + baryte + iron oxide (magnetite, hematite, "limonite") ore deposit located in the NE sector of the Sant'Anna tectonic window, in the southern Apuan Alps, northern Tuscany, Italy [9]. The main orebodies are hosted within the Apuane Unit and, in particular, in a Paleozoic metavolcanic-metasedimentary sequence, locally tourmalinized, and close to the contact with overlying Triassic metadolostone belonging to the "Grezzoni" Formation. The rocks belonging to the Apuane Unit were metamorphosed up to greenschist facies conditions, with *T* and *P* conditions between 350–450 °C and 0.3–0.4 GPa ([10] and references therein). In addition to magnanelliite, the Monte Arsiccio mine is the type locality for eight mineral species: boscardinite [11], protochabournéite [12], arsiccioite [13], mapiquiroite [14], andreadiniite [15], giacovazzoite [4], scordariite [5], and bianchiniite [8].

The sulfate assemblage in which magnanelliite was collected occurs in an old stope of the mine where microcrystalline pyrite is exposed and deeply altered. This ongoing oxidation process has given rise to a large suite of secondary phases [5], among them, several K-Fe³⁺ sulfates: krausite, goldichite, giacovazzoite, scordariite, and the latest addition, magnanelliite.

2.1. Physical Properties

Magnanelliite occurs as steeply terminated prisms, elongated on [100], up to 0.5 mm long, occurring as isolated individuals and in divergent intergrowths (Figure 1). Observed forms are {010}, {001}, {021}, and {1.13.0}. The faces of the {1.13.0} form are typically curved, and may correspond to a combination of several forms, e.g., {190}, {1.11.0}, and {1.13.0}, as reported for alcaparrosaite [16]. The color is yellow to orange-yellow and the streak is pale yellow. Magnanelliite is transparent, vitreous, and displays no fluorescence. The Mohs hardness is ca. 3. The mineral is brittle, with two cleavages: good on {010} and fair on {100}; the fracture is conchoidal to even. Density was measured by sink-float in methylene iodide-toluene. It is 2.82(3) g/cm³, compared with a density of 2.883 g/cm³, calculated on the basis of the empirical chemical formula and the unit-cell volume refined from single-crystal X-ray diffraction data at room temperature.

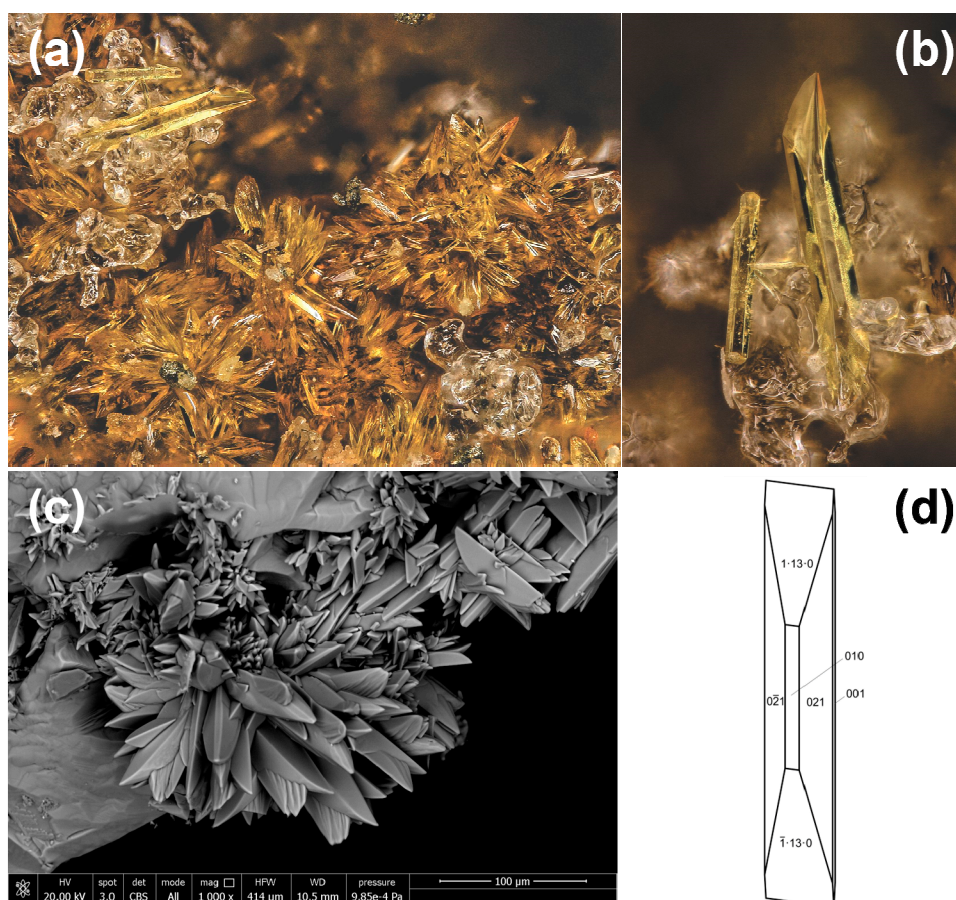


Figure 1. Magnanelliite as (a) divergent intergrowths of steeply terminated prisms (field of view = 1.25 mm) or (b) as isolated individuals (field of view = 0.5 mm), in association with colorless alum-(K). In (c), SEM image showing a divergent intergrowth of magnanelliite. A crystal drawing (clinographic projection in non-standard orientation with a vertical c) of a crystal is shown in (d).

Magnanelliite is optically biaxial (+), with the refraction indices $\alpha = 1.628(2)$, $\beta = 1.637(2)$, $\gamma = 1.665(2)$ (determined in white light), $2V_{\text{meas}} = 60(2)^\circ$, and $2V_{\text{calc}} = 59.9^\circ$. It exhibits strong dispersion, $r > v$. The optical orientation is $Y = \mathbf{b}$, $X \wedge c \approx 25^\circ$ in the obtuse angle β . It is pleochroic, with $X = \text{orange yellow}$, Y and $Z = \text{yellow}$; $X > Y \sim Z$. The compatibility index, calculated using the Gladstone–Dale relationship [17,18], is 0.015 (superior).

In the studied specimens, magnanelliite is associated with alum-(K), giacovazzoite, gypsum, jarosite, krausite, melanterite, and scordariite.

2.2. Chemical and Spectroscopic Data

A preliminary chemical analysis using a FEI Quanta 450 ESEM FEG (FEI Company, Hillsboro, OR, USA) equipped with a QUANTAX Xflash detector 6|10 (EDS mode) (Bruker, Billerica, MA, USA) did not indicate the presence of elements ($Z > 9$) other than K, Fe, and S.

Quantitative chemical data were collected on one polished crystal using a JEOL JXA 8200 electron microprobe (JEOL, Tokyo, Japan) operating in WDS mode at 8 kV and 20 nA, with the beam defocused to 15 μm in diameter to limit sample damage. The slightly high analytical total obtained after addition of calculated H_2O content (on the basis of structural data—see below) is likely due to the partial dehydration of the sample under high vacuum during carbon coating or during electron microprobe analysis. Such a dehydration was manifested by fractures in the sample surface. The following standards (element, emission line) were used: synthetic MgSO_4 ($\text{MgK}\alpha$, $\text{SK}\alpha$), synthetic TiO_2 ($\text{TiK}\alpha$),

albite (AlK α , NaK α), hematite (FeK α), and sanidine (KK α). Chemical data (average of 4 spot analyses) are given in Table 1. Iron is assumed to be trivalent, in agreement with the structural study (see below).

Table 1. Chemical data (in wt.%) for magnanelliite.

Oxide	wt.% (<i>n</i> = 4)	Range	e.s.d.
SO ₃	47.82	46.15–48.59	1.02
TiO ₂	0.05	0.02–0.09	0.02
Al ₂ O ₃	0.40	0.24–0.58	0.05
Fe ₂ O ₃	25.21	24.05–26.17	0.84
MgO	0.07	0.02–0.17	0.02
Na ₂ O	0.20	0.10–0.34	0.04
K ₂ O	21.35	21.08–22.34	0.78
H ₂ O _{calc}	6.85		
Total	101.95		

Note: H₂O was calculated in agreement with structural data. e.s.d. = estimated standard deviation.

The empirical formula of magnanelliite, calculated on the basis of 19 anions per formula unit (pfu), assuming the occurrence of one (OH)[−] and two H₂O groups, is (K_{2.98}Na_{0.04}) Σ 3.02 (Fe³⁺_{2.08}Al_{0.05}Mg_{0.01}) Σ 2.14S_{3.93}O₁₆(OH)(H₂O)₂. The end-member formula of magnanelliite can be written as K₃Fe³⁺₂(SO₄)₄(OH)(H₂O)₂, corresponding to (in wt.%): SO₃ 48.06, Fe₂O₃ 23.97, K₂O 21.21, H₂O 6.76, sum 100.00. Magnanelliite is not soluble in H₂O at room temperature.

Micro-Raman spectra of magnanelliite were obtained on an unpolished sample in nearly back-scattered geometry with a Horiba Jobin-Yvon XploRA Plus apparatus (Horiba France SAS, Longjumeau Cedex, France), equipped with a motorized *x-y* stage and an Olympus BX41 microscope (SPOT Imaging, Sterling Heights, MI, USA) with a 10 \times objective. The 532 nm line of a solid-state laser was used. The minimum lateral and depth resolution was set to a few μ m. The system was calibrated using the 520.6 cm^{−1} Raman band of silicon before each experimental session. Spectra were collected through three acquisitions with single counting times of 180 s, with the laser power filtered at 25% (i.e., 6.25 mW). No thermal damage was observed. Backscattered radiation was analyzed with a 1200 gr/mm grating monochromator. Figure 2 shows the Raman spectrum of magnanelliite. In the region between 400 and 1300 cm^{−1}, bands related to bending and stretching modes of SO₄ groups occur. Symmetrical stretching modes ν_1 occur at 947 and 1001 cm^{−1}, whereas antisymmetric stretching modes ν_3 are at 1074, 1082, 1116, 1157, 1215, and 1240 cm^{−1}. Symmetric bending vibrations ν_2 occur at 372, 435, 474, and 502 cm^{−1}, whereas bands at 576, 606, and 635 cm^{−1} can be attributed to ν_4 antisymmetric bending modes. The band at 848 cm^{−1} can be interpreted as due to librations of H₂O groups, in agreement with previous authors (e.g., [19,20]). Finally, bands at wavenumbers lower than 300 cm^{−1} (147, 206, 243, and 286 cm^{−1}) can be related to lattice vibrations and Fe–O modes. The stretching of O–H bonds, related to the presence of H₂O groups, is represented by relatively weak and broad bands between 3000 and 3600 cm^{−1}.

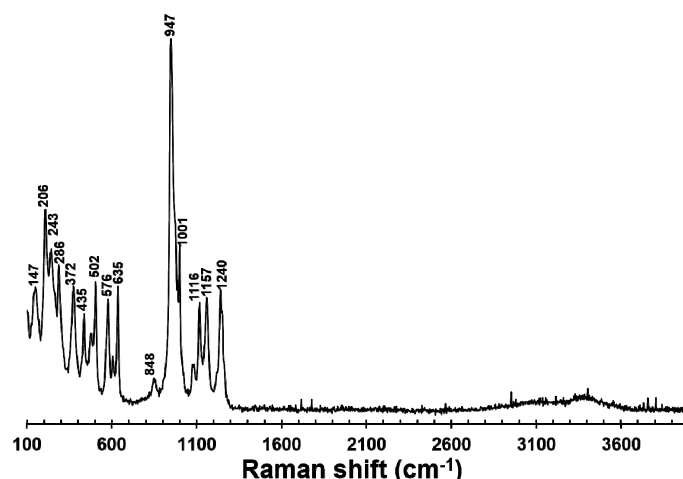


Figure 2. Micro-Raman spectrum of magnanelliite. The position of the main bands is indicated.

2.3. X-Ray Crystallography

X-ray powder diffraction data for magnanelliite (Table 2) were collected using a 114.6 mm Gandolfi camera and Ni-filtered $\text{CuK}\alpha$ radiation. Unit-cell parameters were not refined, owing to the multiple attribution of indices for the strongest reflections.

Table 2. X-ray powder diffraction data (d in Å) for magnanelliite.

I_{obs}	d_{obs}	I_{calc}	d_{calc}	hkl	I_{obs}	d_{obs}	I_{calc}	d_{calc}	hkl
w	8.4	5	8.433	0 2 0	mw	2.597	35	2.601	$\bar{2}$ 4 2
m	6.9	70	6.923	0 2 1	w	2.554	5	2.566	$\bar{1}$ 3 4
		16	6.876	1 1 0	vw	2.476	5	2.466	$\bar{3}$ 1 1
vw	6.1	12	6.155	$\bar{1}$ 1 1	mw	2.410	37	2.416	1 5 3
mw	4.91	40	4.923	0 2 2	vw	2.343	5	2.351	$\bar{2}$ 2 4
w	4.67	34	4.701	$\bar{1}$ 1 2			5	2.331	0 2 5
vw	4.16	5	4.166	1 3 1	vw	2.289	6	2.252	2 6 0
mw	3.612	12	3.692	$\bar{1}$ 3 2	w	2.245	7	2.242	1 1 5
		18	3.645	0 2 3	vw	2.201	6	2.232	$\bar{2}$ 6 1
mw	3.427	31	3.588	$\bar{1}$ 1 3	w	2.103	5	2.108	0 8 0
		21	3.438	2 2 0			7	2.099	1 3 5
mw	3.300	9	3.365	$\bar{2}$ 2 1	w	2.011	12	2.014	$\bar{1}$ 7 3
		28	3.305	$\bar{2}$ 0 2	w	1.966	10	1.968	3 5 1
s	3.085	6	3.253	2 2 1	mw	1.932	6	1.941	3 3 3
		100	3.102	2 0 2			20	1.932	$\bar{1}$ 5 5
		42	3.078	1 5 0	vw	1.879	5	1.879	3 5 2
m	3.006	41	3.074	$\bar{1}$ 3 3	mw	1.837	10	1.845	$\bar{3}$ 5 3
		26	3.032	0 0 4			12	1.836	$\bar{2}$ 0 6
		61	3.005	$\bar{1}$ 5 1	mw	1.719	17	1.719	4 4 0
5	2.963	1 5 1	5	1.712			$\bar{1}$ 5 6		
w	2.838	18	2.843	$\bar{1}$ 1 4	w	1.685	2	1.687	4 4 1
-	-	6	2.768	$\bar{2}$ 4 1			2	1.686	$\bar{2}$ 6 5
-	-	6	2.738	0 6 1			2	1.683	$\bar{2}$ 4 6
m	2.704	28	2.713	1 5 2	w	1.640			
		16	2.707	$\bar{2}$ 2 3	vw	1.596			

Note: intensity and d_{hkl} were calculated using the software PowderCell 2.3 [21] on the basis of the structural model reported in Table 4. Only calculated reflections with $I_{\text{calc}} > 5$ are listed, if not observed. Observed intensities were visually estimated: s = strong; m = medium; mw = medium-weak; w = weak; vw = very weak. The eight strongest reflections are shown in bold.

Single-crystal intensity data were collected using a Bruker AXS Smart Breeze diffractometer (Bruker AXS Inc., Madison, WI, USA) equipped with a Photon II CCD area detector (Bruker, Billerica, MA, USA) and graphite-monochromatized MoK α radiation. The detector-to-crystal distance was 50 mm. Data were collected using ω and φ scan modes, in 0.5° slices, with an exposure time of 30 s per frame. The data were corrected for Lorentz and polarization factors and absorption using the software package Apex3 [22].

The crystal structure of magnanelliite was refined using Shelxl-2018 [23] starting from the atom coordinates of alcaparrosaite [16], with which magnanelliite is isostructural. The following neutral scattering curves, taken from the International Tables for Crystallography [24] were used: K at K(1)-K(3) sites, Fe versus Al at Fe site, S at S(1)-S(3) sites, and O at the O(1)-Ow sites. After several cycles of isotropic refinement, the R_1 converged to 0.0839, indicating the correctness of the structural model. Refining anisotropic displacement parameters for all the atom positions, the R_1 was lowered to 0.0335. The positions of the H atoms were found in the difference-Fourier map. The structural model finally converged to 0.0248 for 2411 reflections with $F_o > 4\sigma(F_o)$ and 144 refined parameters. Details of data collection and refinement are given in Table 3. Atom coordinates and equivalent isotropic or isotropic displacement parameters are reported in Table 4. The crystallographic information file (CIF) of magnanelliite is available as Supplementary material linked to this article.

Table 3. Crystal and experimental details for magnanelliite.

Crystal Data	
Crystal size (mm)	0.170 × 0.040 × 0.030
Cell setting, space group	Monoclinic, C2/c
<i>a</i> (Å)	7.5491(3)
<i>b</i> (Å)	16.8652(6)
<i>c</i> (Å)	12.1574(4)
β (°)	94.064(1)
<i>V</i> (Å ³)	1543.95(10)
<i>Z</i>	4
Data Collection and Refinement	
Radiation, wavelength (Å)	MoK α , 0.71073
Temperature (K)	293
2 θ_{\max} (°)	63.08
Measured reflections	11,078
Unique reflections	2569
Reflections with $F_o > 4\sigma(F_o)$	2411
R_{int}	0.0183
$R\sigma$	0.0161
Range of <i>h, k, l</i>	−11 ≤ <i>h</i> ≤ 10, −24 ≤ <i>k</i> ≤ 23, −13 ≤ <i>l</i> ≤ 17
$R (F_o > 4\sigma(F_o))$	0.0248
R (all data)	0.0268
wR (on F_o^2)	0.0628
Goof	1.147
Number of least-squares parameters	144
Maximum and minimum residual peak ($e \text{ \AA}^{-3}$)	1.06 [at 0.59 Å from K(3)] −0.88 [at 0.91 Å from K(3)]

Table 4. Sites, Wyckoff positions, site occupancy factors (s.o.f.), atom coordinates, and equivalent isotropic or isotropic (*) displacement parameters (\AA^2) for magnanelliite.

Site	Wyckoff Position	s.o.f.	x	y	z	$U_{\text{eq/iso}}$
K(1)	4e	K _{1.00}	0	0.47386(3)	$\frac{3}{4}$	0.01948(11)
K(2)	4c	K _{1.00}	$\frac{1}{4}$	$\frac{3}{4}$	$\frac{1}{2}$	0.01933(11)
K(3)	4e	K _{1.00}	$\frac{1}{2}$	0.38275(4)	$\frac{3}{4}$	0.0555(3)
Fe	8f	Fe _{0.92(1)} Al _{0.08(1)}	0.62274(3)	0.61296(2)	0.63183(2)	0.00974(8)
S(1)	8f	S _{1.00}	0.26061(5)	0.54093(2)	0.50625(3)	0.01191(9)
S(2)	4e	S _{1.00}	0	0.68219(3)	$\frac{3}{4}$	0.01108(10)
S(3)	4e	S _{1.00}	$\frac{1}{2}$	0.77442(3)	$\frac{3}{4}$	0.01165(11)
O(1)	8f	O _{1.00}	0.10021(16)	0.58741(8)	0.49271(12)	0.0224(3)
O(2)	8f	O _{1.00}	0.26489(18)	0.48569(8)	0.59890(10)	0.0198(2)
O(3)	8f	O _{1.00}	0.41708(16)	0.59614(7)	0.51901(10)	0.0168(2)
O(4)	8f	O _{1.00}	0.71804(16)	0.50446(7)	0.59846(10)	0.0158(2)
O(5)	8f	O _{1.00}	0.00565(17)	0.73042(8)	0.65120(11)	0.0192(2)
O(6)	8f	O _{1.00}	0.84128(16)	0.62861(7)	0.73791(10)	0.0171(2)
O(7)	8f	O _{1.00}	0.65733(17)	0.82197(8)	0.77449(12)	0.0206(2)
O(8)	8f	O _{1.00}	0.52637(17)	0.72121(7)	0.65304(10)	0.0180(2)
OH(9)	4e	O _{1.00}	$\frac{1}{2}$	0.56792(10)	$\frac{3}{4}$	0.0196(4)
Ow	8f	O _{1.00}	0.75853(16)	0.66104(8)	0.50743(10)	0.0163(2)
H(1)	8f	H _{1.00}	0.842(4)	0.6932(19)	0.538(3)	0.071(12) *
H(2)	8f	H _{1.00}	0.803(6)	0.6207(19)	0.471(3)	0.093(15) *
H(3)	8f	H _{0.50}	0.598(6)	0.548(4)	0.787(5)	0.053(19) *

3. Crystal Structure Description

Seven independent cation and ten anion sites were located in the crystal structure of magnanelliite. Table 5 reports selected bond distances, and Table 6 gives the bond-valence calculations obtained using the parameters of Brese and O’Keeffe [25] and corrected for H-bonds using the relationship of Ferraris and Ivaldi [26].

Table 5. Selected bond distances (\AA) for magnanelliite.

K(1)	–O(4)	2.7632(12) × 2	K(2)	–O(5)	2.7150(13) × 2	K(3)	–O(7)	2.8179(13) × 2
	–O(2)	2.8167(13) × 2		–O(8)	2.7386(13) × 2		–O(5)	2.8376(15) × 2
	–O(7)	2.8304(14) × 2		–O(3)	2.8872(13) × 2		–O(2)	3.0127(14) × 2
	–O(6)	2.8713(14) × 2		–O(1)	2.9650(14) × 2		–OH(9)	3.1230(19)
	–O(1)	3.1670(14) × 2		–O(7)	3.0343(14) × 2		–O(4)	3.2782(13) × 2
	average	2.8897		average	2.8680		average	3.0018
Fe	–OH(9)	1.9204(7)	S(1)	–O(1)	1.4420(13)	S(2)	–O(5)	1.4538(13) × 2
	–O(8)	1.9888(12)		–O(2)	1.4603(13)		–O(6)	1.4995(12) × 2
	–O(3)	2.0176(12)		–O(3)	1.5035(12)		average	1.4766
	–O(4)	2.0179(12)		–O(4)	1.5039(12)			
	–O(6)	2.0379(12)		average	1.4774	S(3)	–O(7)	1.4464(12) × 2
	–Ow	2.0532(12)					–O(8)	1.5060(12) × 2
	average	2.0060					average	1.4762
Hydrogen bonds (D = donor, A = acceptor)								
D–H	<i>d</i> (D–H)	<i>d</i> (H...A)	D–H...A angle (°)	<i>d</i> (D...A)	A			
Ow–H(1)	0.889(18)	1.89(2)	155(4)	2.7279(18)	O(5)			
Ow–H(2)	0.888(19)	2.31(4)	122(4)	2.8797(18)	O(1)			
Ow–H(2)	0.888(19)	2.04(3)	142(4)	2.7919(18)	O(2)			
OH(9)–H(3)	0.91(3)	1.97(4)	157(6)	2.8259(16)	O(2)			

Table 6. Weighted bond-valence sums (in valence units) for magnanelliite.

	K(1)	K(2)	K(3)	Fe(1)	S(1)	S(2)	S(3)	Σ anions	H Bonds	Σ anions ^a
O(1)	0.06 \downarrow $\times 2$	0.10 \downarrow $\times 2$			1.64			1.80	+0.16	1.96
O(2)	0.16 \downarrow $\times 2$		0.09 \downarrow $\times 2$		1.56			1.81	+0.19 +0.17	2.00 2.17 ^b
O(3)		0.13 \downarrow $\times 2$		0.49	1.38			2.00		2.00
O(4)	0.18 \downarrow $\times 2$		0.04 \downarrow $\times 2$	0.49	1.38			2.09		2.09
O(5)		0.21 \downarrow $\times 2$	0.15 \downarrow $\times 2$			1.58 \downarrow $\times 2$		1.94	+0.21	2.15
O(6)	0.13 \downarrow $\times 2$			0.47		1.40 \downarrow $\times 2$		2.00		2.00
O(7)	0.15 \downarrow $\times 2$	0.09 \downarrow $\times 2$	0.16 \downarrow $\times 2$				1.62 \downarrow $\times 2$	2.02		2.02
O(8)		0.19 \downarrow $\times 2$		0.54			1.38 \downarrow $\times 2$	2.11		2.11
OH(9)			0.07	0.65				1.37	−0.17	1.20
Ow				0.45				0.45	−0.21 −0.19 −0.16	−0.11
Σ cations	1.36	1.44	0.95	3.09	5.96	5.96	6.00			

The BVS has been weighted according to the site occupancy. ^a After correction for H-bonds. ^b When involved in the OH(9)–H(3)···O(2) bond.

Potassium is hosted at three independent sites, K(1), K(2), and K(3). K(1) and K(2) are ten-fold coordinated, whereas K(3) is nine-fold coordinated. However, if one takes into account two additional longer bonds, the K(3) site can be considered as eleven-fold coordinated, as in alcaparrosite [16]. Bond valence sums (BVS) range between 0.95 and 1.44 valence unit (v.u.). The over-bonding at the K(1) and K(2) site is similar to that observed in alcaparrosite, where BVS values of 1.30 and 1.35 v.u. have been reported [16].

Iron is hosted at the octahedrally-coordinated Fe(1) site. Its average bond distance is 2.006 Å, with bond distances ranging between 1.920 and 2.053 Å. The difference between the longest and shortest Fe–O distances, hereafter Δd , is 0.133 Å, compared with 0.2818 Å observed in alcaparrosite, where the occurrence of Ti⁴⁺ increases the octahedral distortion, in agreement with the usual off-center displacement shown by this cation having a small radius and a high charge [27]. The refined site scattering at Fe(1) is 25.0 electrons. Taking into account the chemical data, the site population (Fe_{0.972}Al_{0.023}Mg_{0.005}) can be proposed, corresponding to 25.6 electrons. The BVS is 3.09 v.u., in agreement with the presence of Fe³⁺. In alcaparrosite, where a mixed (Ti⁴⁺_{0.5}Fe³⁺_{0.5}) site occupancy occurs, the corresponding BVS is 3.542 v.u. [16].

Sulfur occurs at three independent S sites, showing S–O distances ranging between 1.442 and 1.506 Å, with <S–O> distances between 1.476 and 1.477 Å. BVS values range between 5.96 and 6.00 v.u.

The examination of the BVS at the O sites reveals the presence of four under-bonded oxygen atoms hosted at O(1), O(2), OH(9), and Ow sites. Indeed, Ow is bonded to two H atoms, i.e., H(1) and H(2), and is an H₂O group. It is donor in the H-bonds with O(5), through H(1), and to both O(1) and O(2), through H(2) (Table 5). In the isostructural mineral alcaparrosite, Kampf et al. [16] took into account only the Ow–H(2)···O(2) bond. However, O(1) remained under-bonded, with a BVS of 1.787 v.u. Likely, H(2) may actually be involved in a bifurcated H-bond with O(1) and O(2). It is worth noting that the Ow–H(2)···O(2) angle is close to the lower limit (~120° [28]), considered as indicative of bonding interactions, whereas the H(2)···O(2) distance, i.e., 2.31(4) Å, is below the 2.5 Å limit, considered as the longest H···A distance in H-bonds [28]. The oxygen atom at the OH(9) site has a BVS of 1.37 v.u. and it is bonded to H(3), statistically occupying a position above and below the mirror plane. In this way, O(2) can also be an acceptor in the OH(9)–H(3)···O(2) bonds. The occurrence of an (OH)[−] group at OH(9) is an important difference with respect to alcaparrosite, where O(9) is occupied by an O^{2−} anion, in agreement with the BVS of 1.882 v.u. [16].

In the crystal structure of magnanelliite, two symmetry-related Fe-centered octahedra are connected through corner-sharing [OH(9) is the shared site], forming a dimer. The opposite vertex is occupied by an H₂O group (Ow site). The four remaining O sites are shared with (SO₄) groups. Along c, dimers are connected through two S(1)-centered tetrahedra. S(3)-centered tetrahedra are bonded to only one

dimer. Tetrahedral-octahedral chains running along *c* are connected along *a* through S(2)-centered tetrahedra, giving rise to undulating {010} layers. Bonding between {010} layers is achieved through three K atoms hosted within the interlayer (Figure 3).

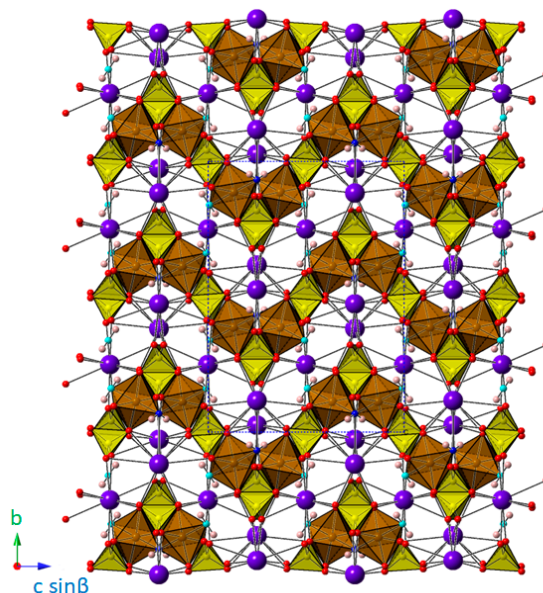


Figure 3. Crystal structure of magnanelliite, as seen down *a*. Symbols: polyhedra represent Fe-centered (brown) and S-centered (yellow) sites. Circles represent H (pink), K (mauve), O (red), OH (blue), and Ow (light blue) sites.

4. Discussion

Magnanelliite is a new addition to the $K_2O-Fe_2O_3-SO_3-H_2O$ quaternary system, currently including the minerals giacovazzoite, goldichite, jarosite, krausite, scordariite, and yavapaiite. It is worth noting that all these species, with the exception of anhydrous yavapaiite, have been observed in the Monte Arsiccio sulfate assemblage, where they likely formed as the result of the interaction between acidic solutions, derived through pyrite oxidation, and K-bearing rocks.

Magnanelliite is related to alcaparrosaitite [16] through the coupled heterovalent substitution $FeTi^{4+} + O^{(9)}O^{2-} = FeFe^{3+} + O^{(9)}OH^-$. Following the definition of mineral groups given by Mills et al. [29], magnanelliite and alcaparrosaitite belong to the same group, having essentially a similar structure and being formed by chemically similar elements. This group can be named the alcaparrosaitite group.

Supplementary Materials: The CIF of magnanelliite is available online at <http://www.mdpi.com/2075-163X/9/12/779/s1>.

Author Contributions: C.B. conceived and designed the experiments; C.B. collected the single-crystal X-ray diffraction and micro-Raman data; A.R.K. collected physical data (density, optical properties); L.B. collected electron-microprobe data; C.B., L.B., and A.R.K. analyzed the data; C.B. wrote the manuscript, with inputs from L.B. and A.R.K.

Funding: This research received support by the University of Pisa through the project P.R.A. 2018–2019 “Georisorse e Ambiente” (Grant No. PRA_2018_41).

Acknowledgments: M. Bianchini provided us with the first specimen of magnanelliite. The manuscript benefited from the comments of two anonymous reviewers.

Conflicts of Interest: The authors declare no conflict of interest.

References

1. D’Achiardi, A. *Mineralogia Della Toscana*; Tipografia Nistri: Pisa, Italy, 1872; Volume 1, 276p.

2. Biagioni, C.; Bonaccorsi, E.; Orlandi, P. Volaschioite, $\text{Fe}^{3+}_4(\text{SO}_4)\text{O}_2(\text{OH})_6 \cdot 2\text{H}_2\text{O}$, a new mineral species from Forno Volaschio, Apuan Alps, Tuscany, Italy. *Can. Mineral.* **2011**, *49*, 605–614. [[CrossRef](#)]
3. Mauro, D.; Biagioni, C.; Bonaccorsi, E.; Hålenius, U.; Pasero, M.; Skogby, H.; Zaccarini, F.; Sejkora, J.; Plášil, J.; Kampf, A.R.; et al. Bohuslavite, $\text{Fe}^{3+}_4(\text{PO}_4)_3(\text{SO}_4)(\text{OH})(\text{H}_2\text{O})_{10} \cdot n\text{H}_2\text{O}$, a new hydrated iron phosphate-sulfate. *Eur. J. Mineral.* **2019**, *31*. [[CrossRef](#)]
4. Biagioni, C.; Bindi, L.; Mauro, D.; Pasero, M. Giacobazzoite, IMA 2018-165. CNMNC Newsletter No. 49. *Eur. J. Mineral.* **2019**, *31*. [[CrossRef](#)]
5. Biagioni, C.; Bindi, L.; Mauro, D.; Hålenius, U. Crystal chemistry of sulfates from the Apuan Alps (Tuscany, Italy). V. Scordariite, $\text{K}_8(\text{Fe}^{3+}_{0.67}\square_{0.33})[\text{Fe}^{3+}_3\text{O}(\text{SO}_4)_6(\text{H}_2\text{O})_3]_2(\text{H}_2\text{O})_{11}$: A new metavoltine-related mineral. *Minerals* **2019**, *9*, 702. [[CrossRef](#)]
6. Bonazzi, P.; Menchetti, S.; Caneschi, A.; Magnanelli, S. Bottinoite, $\text{Ni}(\text{H}_2\text{O})_6[\text{Sb}(\text{OH})_6]_2$, a new mineral from the Bottino mine, Alpi Apuane, Italy. *Am. Mineral.* **1992**, *77*, 1301–1304.
7. Moëlo, Y.; Orlandi, P.; Guillot-Deudon, C.; Biagioni, C.; Paar, W.; Evain, M. Lead-antimony sulfosalts from Tuscany (Italy). XI. The new mineral species parasterryite, $\text{Ag}_4\text{Pb}_{20}(\text{Sb}_{14.5}\text{As}_{9.5})_{\Sigma 24}\text{S}_{58}$, and associated sterryite, $\text{Cu}(\text{Ag},\text{Cu})_3\text{Pb}_{19}(\text{Sb},\text{As})_{22}(\text{As}-\text{As})\text{S}_{56}$, from the Pollone mine, Tuscany, Italy. *Can. Mineral.* **2011**, *49*, 623–638. [[CrossRef](#)]
8. Biagioni, C.; Pasero, M.; Hålenius, U.; Bosi, F. Bianchiniite, IMA 2019-022. CNMNC Newsletter No. 50. *Eur. J. Mineral.* **2019**, *31*. [[CrossRef](#)]
9. Costagliola, P.; Benvenuti, M.; Tanelli, G.; Cortecchi, G.; Lattanzi, P. The barite-pyrite-iron oxides deposit of Monte Arsiccio (Apuane Alps). Geological setting, mineralogy, fluid inclusions, stable isotopes and genesis. *Boll. Soc. Geol. Ital.* **1990**, *109*, 267–277.
10. Molli, G.; Vitale Brovarone, A.; Beyssac, O.; Cinquini, I. RSCM thermometry in the Alpi Apuane (NW Tuscany, Italy): New constraints for the metamorphic and tectonic history of the inner northern Apennines. *J. Struct. Geol.* **2018**, *113*, 200–216. [[CrossRef](#)]
11. Orlandi, P.; Biagioni, C.; Bonaccorsi, E.; Moëlo, Y.; Paar, W.H. Lead-antimony sulfosalts from Tuscany (Italy). XII. Boscardinite, $\text{TiPb}_4(\text{Sb}_7\text{As}_2)_{\Sigma 9}\text{S}_{18}$, a new mineral species from the Monte Arsiccio mine: Occurrence and crystal structure. *Can. Mineral.* **2012**, *50*, 235–251. [[CrossRef](#)]
12. Orlandi, P.; Biagioni, C.; Moëlo, Y.; Bonaccorsi, E.; Paar, W. Lead-antimony sulfosalts from Tuscany (Italy). XIII. Protochabournéite, $\sim\text{Ti}_2\text{Pb}(\text{Sb}_{9.8}\text{As}_{1.2})_{\Sigma 10}\text{S}_{17}$, from the Monte Arsiccio mine: Occurrence, crystal structure and relationship with chabournéite. *Can. Mineral.* **2013**, *51*, 475–494. [[CrossRef](#)]
13. Biagioni, C.; Bonaccorsi, E.; Moëlo, Y.; Orlandi, P.; Bindi, L.; D’Orazio, M.; Vezzoni, S. Mercury-arsenic sulfosalts from the Apuan Alps (Tuscany, Italy). II. Arsiccioite, $\text{AgHg}_2\text{TiAs}_2\text{S}_6$, a new mineral from the Monte Arsiccio mine: Occurrence, crystal structure and crystal chemistry of the routhierite isotopic series. *Mineral. Mag.* **2014**, *78*, 101–117. [[CrossRef](#)]
14. Biagioni, C.; Orlandi, P.; Pasero, M.; Nestola, F.; Bindi, L. Mapiquiroite, $(\text{Sr},\text{Pb})(\text{U},\text{Y})_2(\text{Ti},\text{Fe}^{3+})_{18}\text{O}_{38}$, a new member of the crichtonite group from the Apuan Alps, Tuscany, Italy. *Eur. J. Mineral.* **2014**, *26*, 427–437. [[CrossRef](#)]
15. Biagioni, C.; Moëlo, Y.; Orlandi, P.; Paar, W.H. Lead-antimony sulfosalts from Tuscany (Italy). XXIII. Andreadiniite, $\text{CuAg}_7\text{HgPb}_7\text{Sb}_{24}\text{S}_{48}$, a new oversubstituted (Cu,Hg)-rich member of the andorite homeotypic series from the Monte Arsiccio mine, Apuan Alps. *Eur. J. Mineral.* **2018**, *30*, 1021–1035. [[CrossRef](#)]
16. Kampf, A.R.; Mills, S.J.; Housley, R.M.; Williams, P.A.; Dini, M. Alcaparrosite, $\text{K}_3\text{Ti}^{4+}\text{Fe}^{3+}(\text{SO}_4)_4\text{O}(\text{H}_2\text{O})_2$, a new hydrophobic Ti^{4+} sulfate from Alcaparrosa, Chile. *Mineral. Mag.* **2012**, *76*, 851–861. [[CrossRef](#)]
17. Mandarino, J.A. The Gladstone-Dale relationship. Part III. Some general applications. *Can. Mineral.* **1979**, *17*, 71–76.
18. Mandarino, J.A. The Gladstone-Dale relationship. Part IV. The compatibility concept and its application. *Can. Mineral.* **1981**, *19*, 441–450.
19. Frost, R.L.; López, A.; Scholz, R.; Wang, L. A Raman and infrared spectroscopic study of the sulphate mineral aluminite $\text{Al}_2(\text{SO}_4)(\text{OH})_4 \cdot 7\text{H}_2\text{O}$. *Spectrochim. Acta Part A Mol. Biomol. Spectrosc.* **2015**, *148*, 232–236. [[CrossRef](#)]
20. Buzatu, A.; Dill, H.G.; Buzgar, N.; Damian, G.; Maftei, A.E.; Apopei, A.I. Efflorescent sulfates from Baia Sprie mining area (Romania)—Acid mine drainage and climatological approach. *Sci. Total Environ.* **2016**, *542*, 629–641. [[CrossRef](#)]

21. Kraus, W.; Nolze, G. PowderCell—A program for the representation and manipulation of crystal structures and calculation of the resulting X-ray powder patterns. *J. Appl. Crystallogr.* **1996**, *29*, 301–303. [[CrossRef](#)]
22. Bruker AXS Inc. APEX 3. In *Bruker Advanced X-ray Solutions 2016*; Bruker AXS Inc.: Madison, WI, USA, 2016.
23. Sheldrick, G.M. A short history of SHELX. *Acta Crystallogr.* **2008**, *A64*, 112–122. [[CrossRef](#)] [[PubMed](#)]
24. Wilson, A.J.C. (Ed.) *International Tables for Crystallography. Volume C: Mathematical, Physical and Chemical Tables*; Kluwer Academic Publishers: Dordrecht, The Netherlands, 1992.
25. Brese, N.E.; O’Keeffe, M. Bond-valence parameters for solids. *Acta Crystallogr.* **1991**, *B47*, 192–197. [[CrossRef](#)]
26. Ferraris, G.; Ivaldi, G. Bond valence vs bond length in O···O hydrogen bonds. *Acta Crystallogr.* **1988**, *B44*, 341–344. [[CrossRef](#)]
27. Megaw, H.D. A simple theory of the off-center displacement of cations in octahedral environments. *Acta Crystallogr.* **1968**, *B24*, 149–153. [[CrossRef](#)]
28. Brown, I.D. On the geometry of O–H···O hydrogen bonds. *Acta Crystallogr.* **1976**, *A32*, 24–31. [[CrossRef](#)]
29. Mills, S.J.; Hatert, F.; Nickel, E.H.; Ferraris, G. The standardization of mineral group hierarchies: Application to recent nomenclature proposals. *Eur. J. Mineral.* **2009**, *21*, 1073–1080. [[CrossRef](#)]



© 2019 by the authors. Licensee MDPI, Basel, Switzerland. This article is an open access article distributed under the terms and conditions of the Creative Commons Attribution (CC BY) license (<http://creativecommons.org/licenses/by/4.0/>).